LM-05K045
April 19, 2005

The Mechanism and Modeling of Intergranular Stress Corrosion Cracking of Nickel-Chromium-Iron Alloys Exposed to High Purity Water

G Young, W Wilkening, D Morton, E Richey, N Lewis

NOTICE

THE MECHANISM AND MODELING OF INTERGRANULAR STRESS CORROSION CRACKING OF NICKEL-CHROMIUM-IRON ALLOYS EXPOSED TO HIGH PURITY WATER

George A. Young, Weldon W. Wilkening, David S. Morton, Edward Richey, and Nathan Lewis

Lockheed Martin Incorporated
P.O. Box 1072,
Schenectady, NY 12301-1072

Keywords: Nickel Based Alloys, Alloy 600, X-750, Stress Corrosion Cracking, Heat Affected Zone, Hydrogen, Oxygen

Abstract

This investigation combines microstructural characterization, fracture mechanics analyses, atomistic modeling, and experimental crack growth rate data to better elucidate the mechanism of stress corrosion cracking of nickel-based alloys exposed to high temperature, high purity deaerated water. Additionally, this paper develops a mechanistically based equation that is suggested to be generally applicable to SCC of Alloy 600-type alloys exposed to high purity water. Results show that stress corrosion crack tips are truly intergranular, sharp (~5-10 nm crack tip openings), and are well described by moving crack fracture mechanics. These findings, combined with the clear dependency of the crack growth rate on the electrochemical potential and the constancy of the apparent activation energy (see Morton's paper in these proceedings) suggest that the stress corrosion crack growth rate in high purity water is governed by the supply rate of an embrittling species to the crack tip process zone and by the tearing resistance of the material immediately in front of the crack tip (i.e. the local *J-R* curve). Consideration of both hydrogen and oxygen embrittlement show that both mechanisms are feasible, although there is somewhat more support for a hydrogen mechanism. An example of the crack growth rate model and data fitting procedures are given for Alloy 600 heat affected zone (HAZ) material. Results show that the fitting procedure can have a large effect on model parameters and subsequent extrapolations. For the data considered, nonlinear curve fitting in real space (vice log space) resulted in the most accurate fit. The Alloy 600 HAZ modeling shows that the apparent activation energy for crack growth is lower than is typically reported (91.2 kJ/mol ± $27.4|_{95\%}$ kJ/mol vice ~130 kJ/mol), the crack growth rate is weakly dependent on the applied stress intensity factor (SCCGR $\propto K^{I}$), and the effect of electrochemical potential is significant (~3.6X near Ni/NiO).

Introduction

Stress corrosion cracking is often thought of as a periodic process in which crack advance occurs discontinuously, after some critical event *e.g.* oxide rupture [1, 2], achievement of a critical hydrogen concentration in front of a crack tip [3], or accumulation of a critical crack tip strain [4, 5]. However, this view of periodic crack growth is at odds with some experimental observations. The relatively small stress corrosion crack tip opening displacements (CTOD's) on the order of 10-100 nm that have been reported for nickel-based alloys [6, 7], β-titanium alloys [8], and 7XXX series aluminum alloys [9, 10] are an order of magnitude or more smaller than what static crack fracture mechanics predicts [11]. This observation suggests the scenario of periodic crack advance with periods of crack arrest and damage accumulation does not accurately describe stress corrosion in these systems. Instead, the crack front may move continuously, via stable intergranular tearing, and moving crack fracture mechanics may be a promising basis for developing an equation for predicting stress corrosion cracking rates [12].

The purposes of the present work are to: (1) better understand the potential mechanism or mechanisms of crack growth and (2) to develop a fundamentally based equation that accurately describes experimental crack growth data and can be used to extrapolate data with confidence. Analytical electron microscopy is used to characterize nickel base alloy stress corrosion cracks produced in high temperature, high purity water. The experimental data are compared to fracture mechanics predictions and novel first-principles atomistic modeling is used to investigate oxygen diffusion in nickel. These experimental and analytical findings are used to assess potential SCC mechanisms and to develop a mechanistically based crack growth rate equation.

Experimental and Computational Methods

Crack Growth Rate Testing

Crack growth rate testing was conducted in high purity, high temperature water, consistent with previous studies [13, 14]. Each crack growth rate reported was from a compact tension-type sample, exposed to a single condition (i.e. constant load, temperature, and electrochemical potential). The reported crack growth rates were determined by physically measuring the crack length and not by correlation with instrumentation. Results are given for both X-750 HTH and for Alloy 600 Heat Affected Zone (HAZ) material. The X-750 testing was done to explore the effect of a hydrogen isotope on the crack growth rate while the Alloy 600 HAZ testing was done to develop a crack growth rate model as a function of stress intensity factor (*K*), temperature (*T*), and electrochemical potential (*EcP*). Additional details of the Alloy 600 heat affected zone (HAZ) testing are given in Reference [14].

The primary sample investigated via electron microscopy was a bolt-loaded, fatigue-precracked compact-tension sample of Alloy 600 in the mill-annealed condition. After precracking in air, the sample was loaded to a stress intensity factor of 27.5 MPa√m and then exposed to high purity, hydrogen-deaerated (40 scc H_2/kg H_2O), 360°C water for ~2.4 years. During SCC testing, the crack grew approximately 315 μm to a final stress intensity factor of ~17.6 MPa√m. For brevity, the starting crack will be referred to as the "fatigue precrack" although it should be highlighted that this crack was monotonically loaded to a stress intensity factor of 27.5 MPa√m and no longer represents purely fatigue loading. After SCC testing, the sample was ground to near the mid-plane and metallographically polished while bolt-loaded and the SCC crack was examined via electron backscatter diffraction (EBSD). After the EBSD examinations were complete, TEM foils were prepared from the areas previously examined via EBSD.

Electron Microscopy

The instrument used to collect the electron backscattered diffraction patterns was a CamScan SC44 SEM, with a tungsten filament and a Hamamatsu camera and image processor. The samples investigated were metallographically polished to a 0.05 μm finish. Samples were tilted approximately 70° from horizontal to maximize signal collection. The EBSD pattern was recorded with a phosphor-based detector, converted into a digital signal, and indexed with commercially available software. Crack tip TEM foils were prepared by mechanical sectioning, mechanical grinding, and ion milling, as described previously [6]. The TEM foils were examined with a Philips CM 300 instrument, equipped with a LaB_6 filament operated at 300 keV.

Atomistic Modeling

First-principles atomistic modeling was used to investigate the diffusivity of oxygen in nickel. All calculations were performed by Materials Design Inc, using the Vienna Ab Initio Simulation Package (VASP). The geometry considered was a 2x2x2 supercell of nickel containing 32 nickel atoms and one oxygen atom. Total energies, forces, and energy profiles are described by *ab initio* quantum mechanics, on the basis of density functional theory (DFT) [15, 16] using the generalized gradient approximation (GGA) [17, 18]. The Kohn-Sham equations of DFT were solved using projector-augmented-wave (PAW) potentials and a plane-wave variational basis set [19]. The equilibrium and transition state structures were determined by a conjugate gradient minimization technique. In the case of energy minima, both the total energies and the forces on the atoms were minimized. Once the equilibrium sites and transition state geometries were determined, the temperature dependent thermodynamic functions (i.e. entropy, enthalpy, and free energy) were determined from phonon calculations using the direct approach developed by K. Parlinski [20].

Results and Discussion

Electron Microscopy

A backscattered SEM image of the A600 fatigue/SCC region is shown in Figure 1. The red arc in front of the fatigue precrack is an estimate of the plane strain plastic zone of the initial crack, as calculated from the parameters in Table I. Note that the SCC crack grew ~2X longer than the initial monotonic plastic zone. The fatigue precrack is at the top of Figure 1 and the SCC crack grew from top to bottom. The boxes in Figure 1 define the three regions investigated via EBSD, which are shown in Figure 2.

Figure 2 compares the grain boundary map (left), the Euler angle image (center), and the misorientation maps (right) for the three regions defined in Figure 1. The red lines in the grain boundary map show boundaries greater than 1.5°, while a relative measure of the strain in the sample is shown in the misorientation map, with low strains shown in blue and high strains shown in red, as indicated by the key in Figure 3. Note the large strain region in front of the fatigue precrack and the lesser, but significant, strains in the plastic zone and intermittently along the stress corrosion crack.

The stress corrosion crack tip strain distribution is compared with a region away from the crack tip but within the initial plastic zone in Figure 4. Notably, there is no apparent increase in strain along the SCC crack or ahead of the crack tip relative to the rest of the plastic zone. While SCC may favor cracking along grain boundaries with accumulated plastic strain (i.e. boundaries with that are shaded green in Figure 2), there is no apparent increased strain along the crack wake or in front of the SCC crack. The EBSD data are in agreement with the extensive TEM work of Lewis *et al.*, which also show that, while the plastic zones of SCC crack tips contain significant strain, there is no consistent increased dislocation density in the SCC wake or ahead of the crack tip (see Figures 5 and 6) [6, 7, 21]. These findings indicate that SCC does not require an increased strain (beyond what is already present in the plastic zone) for crack advance to occur. The implication of this statement is that environmental variables may have a stronger influence on stress corrosion crack growth rates than mechanical variables and that environmental variables such as embrittler supply rate may, in fact, be rate limiting.

Table I. *Parameters used to estimate the plastic zone size in the A600 SCC sample*

Parameters (Mill Annealed A600)	**Constant Load Plane Strain**
True σ_{YS} = 2.55x10^8 Pa	$r_p \approx \frac{1}{6\pi}\left(\frac{K_I}{\sigma_{flow}}\right)^2$
True σ_{UTS} =7.53 x 10^8 Pa	
True σ_0 =5.04 x 10^8 Pa	
K_I = 27.5 MPa$\sqrt{m}$	
Plastic zone radius	152 μm
Extent of SCC	315 μm
Extent of SCC / Plastic Zone Radius	**~2X**

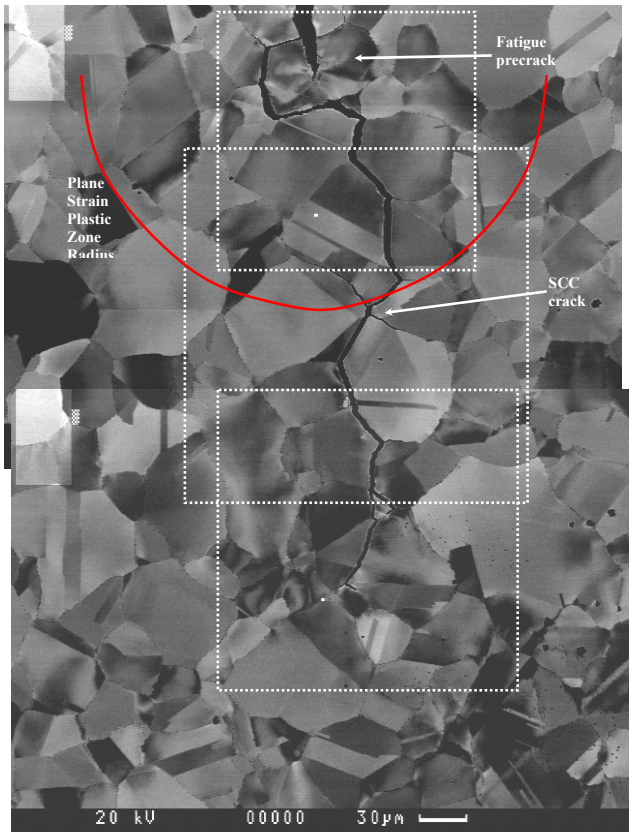

Figure 1. *Electron backscatter SEM image of the plane of the SCC crack that was investigated. The white squares outline the regions investigated via EBSD (Figure 2).*

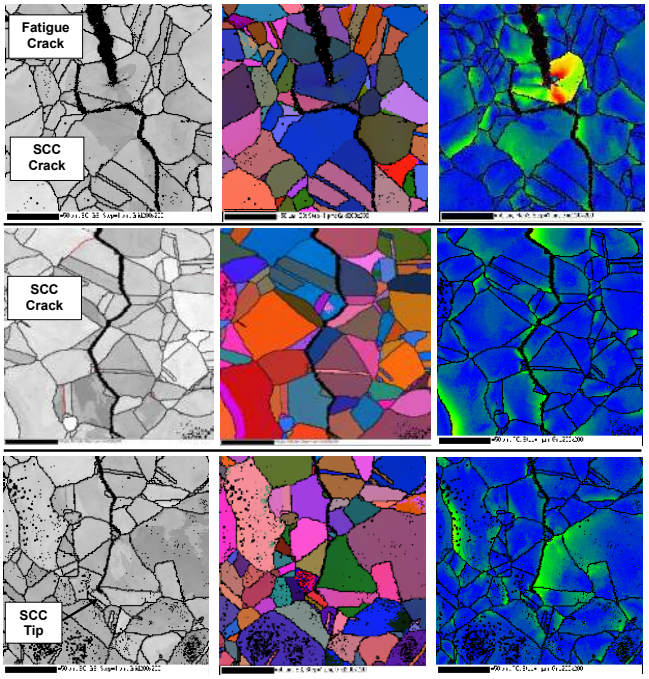

Figure 2. *Comparison of the A600 grain boundary maps (left), Euler angle images (center), and misorientation maps (right) for the three regions investigated. Note the distinct difference in strain between the fatigue crack tip and the SCC tip regions.*

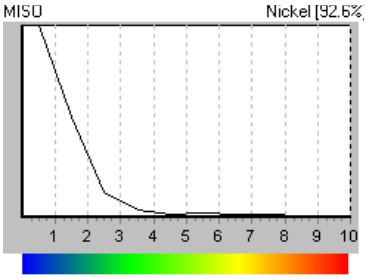

Figure 3. *Relative intragranular misorientation, illustrating the degree of plastic strain in the metal from low (blue) to high (red).*

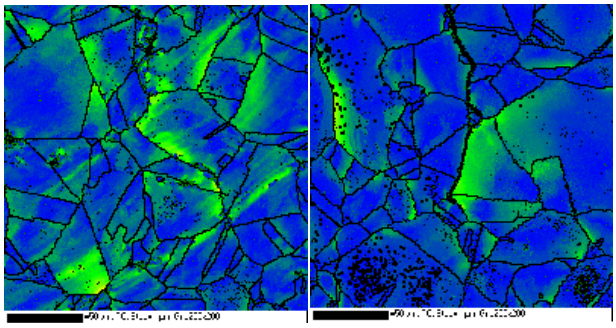

Figure 4. *Comparison of the A600 grain boundary maps for a region in the original plastic zone but away from the SCC crack (left) and the SCC crack tip region (right). Note that the degree of plastic strain is similar between the two.*

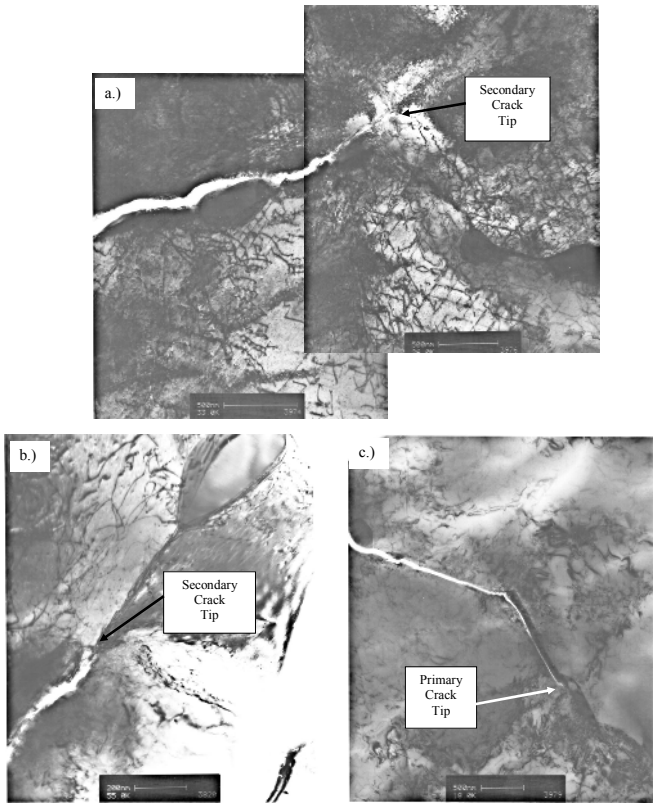

Figure 5. *TEM of A600 SCC crack tip regions. Figures a.) and b.) are secondary cracks, in the wake of the main crack. Figure c.) is from the tip of the primary crack. Note the variation in dislocation density along the crack wakes, consistent with the misorientation maps shown in Figure 2. Additionally, there is no increased strain gradient in front of the SCC crack tips.*

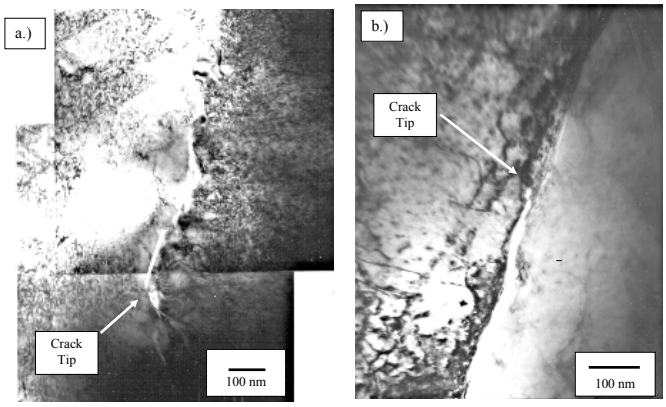

Figure 6. *Comparison of crack tip geometry of the same heat of X-750 AH. a.) stress corrosion cracking (338°C, 50 scc/kg H_2, K=27.5 MPa√m and b.) stress corrosion cracking (338°C, 50 scc/kg H_2, K=49 MPa√m).*

The Analysis of Wilkening

In describing a fracture process such as stress corrosion cracking, Wilkening first differentiates between stable and unstable fracture. Noting that electron microscopy reveals very sharp crack tips – on the order of 1-10 nm (see Figures 5 and 6, which show typical SCC crack tips for X-750 in the AH heat treatment and Alloy 600 in the mill annealed condition), he surmised that cracking occurs stably and continuously on a scale that controls the crack tip morphology. Furthermore, he asserted that moving crack fracture mechanics and the concept of a *J-R* curve local to the crack tip process zone could be used to develop a crack growth rate equation to fit and predict SCC rates.

As a test of this hypothesis, the analysis of Rice, Drugan, and Sham (RDS) [12] was used to predict the CTOD of a moving crack in an elastic perfectly-plastic material. While nickel-based alloys are far from perfectly-plastic when tested in inert environments, an embrittling species such as hydrogen or oxygen could act to embrittle the fracture process zone and make the RDS analysis applicable. Starting with the Rice-Drugan-Sham expression for crack tip opening displacement rate, $\dot{\delta}$:

$$\dot{\delta} = \alpha \frac{\dot{J}}{\sigma_0} + \beta \frac{\sigma_0}{E} \dot{a} \ln\left(\frac{R}{r}\right) \quad for\ r \to 0 \tag{1}$$

and noting that $J = f(a, t)$, it follows that:

$$\dot{J} \equiv \frac{dJ}{dt} = \frac{dJ}{da} \cdot \frac{da}{dt} = \frac{dJ}{da} \cdot \dot{a} \tag{2}$$

Combining Equations (1) and (2) produces the following expression:

$$\dot{\delta} = \left[\frac{\alpha}{\sigma_0} \frac{dJ}{da} + \beta \frac{\sigma_0}{E} \ln\left(\frac{R}{r}\right) \right] \dot{a} \tag{3}$$

Integration of Equation (1), combined with Equation (2), and noting that $da = dr$, yields the following expression for the crack tip opening displacement:

$$CTOD \equiv \delta = \left[\frac{\alpha}{\sigma_0} \frac{dJ}{da} + \beta \frac{\sigma_0}{E} \ln\left(\frac{eR}{r}\right) \right] r, \ as\ r \to 0 \tag{4}$$

Equation (4) was used in conjunction with the parameters given in Table II to predict the crack tip opening displacement for both mill annealed Alloy 600 and for X-750 in the AH heat treatment. Experimentally, the analytical electron microscopy work of Lewis was used to determine the actual CTOD's [7, 21]. The experimental CTOD's, moving crack predictions, and static crack predictions (as per Shih [11]) are compared in Figure 7. Note that (1) the initial fatigue precrack is well predicted by the static crack CTOD, but that both the Alloy 600 and X-750 stress corrosion cracks are much better predicted by a moving crack in an elastic perfectly plastic material.

Similar to what is shown here for nickel-based alloy stress corrosion crack tips, relatively sharp (10-100 nm) crack tip opening displacements of stress corrosion cracks have also been observed for β-titanium alloys [8], and 7XXX series aluminum alloys [9, 10]. In each of these cases, the stress corrosion cracking mechanism is consistent with intergranular embrittlement (likely by corrosion generated hydrogen) [8, 10, 22]. This similarity suggests that SCC of nickel based alloys exposed to high purity water may also occur via intergranular embrittlement. Selected mechanisms of embrittlement are discussed in the following section.

Table II. *Summary of the Parameters Used in Calculating the Crack Tip Opening Displacements*

	Mill Annealed A600 Stress Corrosion Cracking T=680°F (360°C)	**X-750 AH Stress Corrosion Cracking T=640°F (338°C)**
n	(0.05-0.2)	0.2
α **(static crack, plane strain)** **(static crack, perfectly plastic)**	 0.25 0.75	 0.25 0.75
β	5.083	5.083
λ	0.1	0.1
True σ_{YS} (Pa)	(2.55×10^8)	7.20×10^8
True σ_{UTS} (Pa)	(7.53×10^8)	1.34×10^9
True σ_0 (Pa)	(5.04×10^8)	1.03×10^9
E (Pa)	(1.97×10^{11})	1.98×10^{11}
σ_0/E	(2.56×10^{-3})	5.20×10^{-3}
$\delta = (d_n \cdot J/\sigma_0)$	2.0×10^{-6} m K= 27 MPa√m	$(1\text{-}13) \times 10^{-6}$ m for K 25-80 MPa√m
Typical CGR (m/s)	8.8×10^{-11} (0.3 mils/day)	2.3×10^{-10} (1 mil/day)
CTOD, measured 10 nm behind crack tip	$5\text{-}7 \times 10^{-9}$	7×10^{-9}
CTOD predicted (Equation 4), dJ/da = 10, r=10 nm behind tip, *K* = 27 MPa√m	4.0×10^{-9}	$(7.5\text{-}8.0) \times 10^{-9}$
CTOA (measured) (radians)	~(0.05-0.17)	~(0.10-0.20)

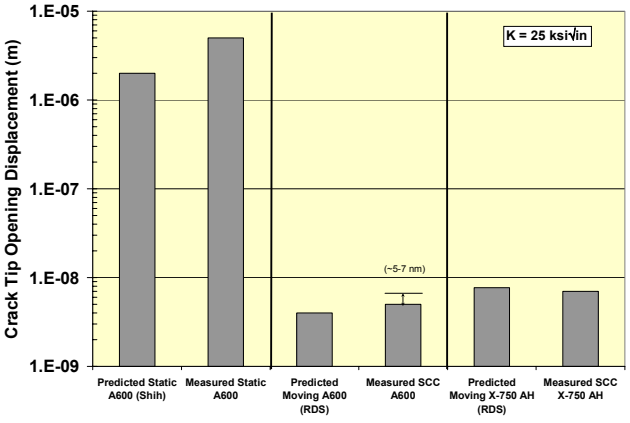

Figure 7. *Comparison of predicted and measured crack tip opening displacements for static and moving cracks. This initial fatigue precrack is blunted, consistent with static crack predictions, but both Alloy 600 and X-750 SCC crack are sharp, consistent with a moving crack in an elastic perfectly-plastic material.*

Mechanisms of SCC

Corrosion

While corrosion is a necessary component of stress corrosion cracking, available data (albeit limited) indicate that the temperature dependence of corrosion of nickel based alloys exposed to high purity water is too low to be the rate controlling process for crack growth. The temperature dependence for crack growth is often shown to be ~130 kJ/mol [23, 24], although the present study suggests a value ~91.2 kJ/mol ± 27.4 kJ/mol is more appropriate (see the section *Application of the Model – SCC of an Alloy 600 HAZ)*. The data of Rosecrans and Duquette report a temperature dependence of corrosion ~37.3 kJ/mol [24], while the data of Brucelle et al. on Inconel 718 suggest a slightly higher temperature dependence of ~67.0 kJ/mol [25]. The various reported temperature dependencies of corrosion of nickel and nickel-based alloys are summarized in Table III.

Table III. *Summary of Activation Energies for Selected Processes in Nickel and Nickel Alloys*

Process	Activation Energy (kJ/mol)	Notes
Corrosion	37.3 67.0	Alloy 600 Bulk Film [24] Inconel 718 [25]
Hydrogen Uptake	15.8-21.0	For Ni-base alloys exposed to hydrogen gas [26, 27]
Hydrogen Diffusion	39.3 42.4-49.8 53.0	Nickel [28] A600 [26, 29] X-750 [26]

Hydrogen Embrittlement

It is notable that several researchers have reported increased hydrogen concentrations near stress corrosion cracks of nickel-based alloys [30-32] and stainless steels [30] exposed to high purity water. However, these experiments lack the spatial resolution to determine if hydrogen actually collects in front of a stress corrosion crack tip and causes stress corrosion or if it is simply the result of the reduction of water (in the crack wake) balancing the oxidation of the alloy (at the crack tip).

In a attempt to assess if hydrogen embrittlement plays a causal role in nickel alloy SCC in high purity water, the Authors have conducted SCC testing on a single heat of X-750 in the HTH heat treatment in both light and heavy water at constant temperature, stress intensity factor, and hydrogen concentration. The purpose behind these tests was to assess if the mass isotope effect for hydrogen diffusion would influence the crack growth rate. As shown in Figure 8, the test conducted in deuterated water was ~1.6X slower than the average crack growth rate from tests conducted in light water, which is in good agreement with the expected 1.4X (i.e. $\sqrt{2}$) decrease in rate. While this observation is consistent with a hydrogen embrittlement based mechanism of SCC, corrosion studies on stainless steels in deuterated water have shown [33] more protective oxide films form in heavy water than in light water, which confounds any definitive conclusion on mechanism.

Another important discriminator for a hydrogen embrittlement based mechanism of cracking is the apparent temperature dependence. Similar to corrosion, the temperature dependencies of hydrogen uptake (~15.8-21.0 kJ/mol) or diffusion (42.4-49.0 kJ/mol for Alloy 600) are too low to account for the observed activation energy of high temperature SCC (again, often reported to be ~130 kJ/mol, but shown here to be 91.2 kJ/mol ± 27.4 kJ/mol).

One way of rationalizing a larger temperature dependence is if hydrogen affects some other process, such as creep. Hall and Symons have constructed a detailed model of stress corrosion cracking based on hydrogen assisted creep fracture [4, 5, 34]. However, experimental support for hydrogen assisted creep fracture is limited and is inconsistent with some of the present findings. As shown by extensive crack tip TEM in this study and in others [6, 7, 21], the stress corrosion crack path of nickel-based alloys exposed to high purity water is truly intergranular along the crystallographic grain boundary and not along a slip plane in the vicinity of the grain boundary [6, 7, 35, 36]. The implication of the intergranular crack path is that decohesion, not enhanced plasticity is likely responsible for crack extension [37-39]. Additionally, neither crack tip TEM nor EBSD reveal an increased strain gradient (*i.e.* a creep fracture zone) ahead of stress corrosion crack tips, which is further indication that cracking occurs in a relatively brittle fashion. Lastly, as discussed by Morton in these proceedings, the apparent activation energy for crack growth is relatively constant and insensitive to changes in applied stress intensity factor, yield strength, or carbon level – all of which are at odds with the present formulation of the HACF model [4, 40]. These observations indicate that intergranular decohesion is the likely mechanism of stress corrosion cracking of nickel alloys exposed to high temperature, high purity water [39].

Another way to explain the temperature dependence of a hydrogen-based mechanism is if the rate controlling process is not simply mass transport, but is the combined process of the hydrogen supply rate (*i.e.* the effective permeability, where $Q_{effective} = Q_{corrosion} + Q_{solution} + Q_{diffusion}$). Taking average values for Alloy 600 from Table III yields an effective activation energy of ~102 kJ/mol, which is in good agreement with the 91.2 kJ/mol ± 27.4 kJ/mol determined in the present study. The concept of embrittler supply rate limited fracture is further developed into a mechanistically based equation.

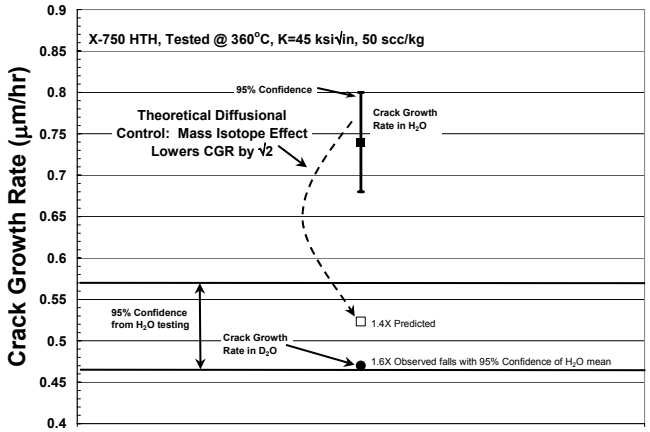

Figure 8. *Comparison of SCC tests conducted on a single heat of X-750 in the HTH heat treatment in light water (filled square) and in heavy water (D_2O). The test in D_2O displayed a 1.6X slower crack growth rate than the average of tests conducted in light water, consistent with the mass isotope effect on hydrogen diffusion (1.4X).*

Oxygen Embrittlement

Scott et al., have done the most extensive work on assessing the feasibility of an internal oxidation or oxygen embrittlement based mechanism of stress corrosion cracking [41-46]. In contrast to corrosion and hydrogen embrittlement, it has been argued that the temperature dependence of oxygen diffusion is too high for oxygen embrittlement to be a viable mechanism for SCC in high temperature water [42, 47]. While there is large scatter in the reported activation energies for oxygen diffusion in nickel, which range between 160-410 kJ/mol, these values are well above the ~130 kJ/mol typically reported for stress corrosion cracking [42, 47-55] and the 91.2 kJ/mol ± 27.4 kJ/mol determined in the present study. However, experimental determination of oxygen diffusion in nickel is extremely difficult and is complicated by the relatively low solubility, the potential presence of oxide films, complications due to chemical reaction, and by microstrucutural trapping. For these reasons a first-principles atomistic study of oxygen diffusion in nickel was performed.

While diffusion studies via first principles are relatively new, recent work has shown excellent agreement with experimental studies [56-58]. The good agreement between an experimental best fit (solid line) [28] and the first principles modeling prediction (dashed line) is shown in Figure 9. Hydrogen diffusion in nickel was chosen as a test case since there are excellent agreement among experimental data [28]. The energetics of oxygen transport in nickel from the first-principles modeling is shown in Figure 10. Taking oxygen substituted on the nickel lattice as a reference, it takes 145.9 kJ/mol to move into an adjacent octahedral site, 96.2 kJ/mol to move into a tetrahedral interstice (196.1-99.9 kJ/mol), and 56.1 kJ/mol to move back into an octahedral interstice far from a vacancy (196.1-140 kJ/mol).

Comparisons of the experimental activation energies for oxygen diffusion in nickel (blue lines) and two diffusion mechanisms from the atomistic modeling study (red lines) are given in Figure 11. The upper red line illustrates the activation energy to move oxygen from a vacancy across the octahedral/tetrahedral transition state (196.1 kJ/mol). These results lend some support to the low temperature Zholobov data [53] and the Park and Alstetter data [54] if excess vacancies are present (as expected near corroded surfaces). However, these activation energies are still significantly higher than the 91.2 kJ/mol found in the present study (or the ~130 kJ/mol typically reported for SCC [23, 24]). Given that interstitial occupancy and diffusion are unlikely in the ~530 K - 630 K range of interest, these findings suggest that if oxygen embrittlement is a feasible mechanism of SCC, grain boundary diffusion is the most likely transport mechanism.

Development of a Crack Growth Rate Equation

Regardless of whether a hydrogen based or oxygen based mechanism is operative, available evidence indicates that the SCC of Alloy 600-type nickel alloys exposed to high purity water is consistent with intergranular decohesion, where the crack growth rate is limited by the embrittler supply rate. Crack advance occurs because the toughness of the metal in front of the crack tip is degraded after exposure to an aggressive environment (i.e. when $J_{applied} = J_{IC}$). The observed SCC rate is a balance between the mechanical driving forces for crack advance (*i.e.* the applied J), the resistance of the material to crack extension, T_{mat}, and the rate of environmental damage. This hypothesis is discussed relative to experimental observations of SCC of A600-type alloys in Table IV and developed into a crack growth rate equation.

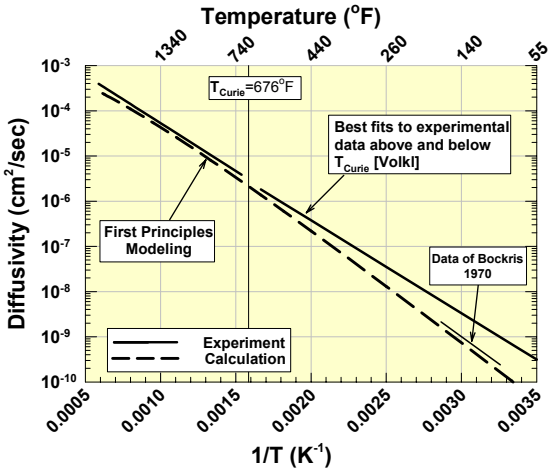

Figure 9. *Comparison of first-principles modeling predictions (dashed line) and experimental data (solid lines) for hydrogen diffusion in nickel, showing good agreement between the two.*

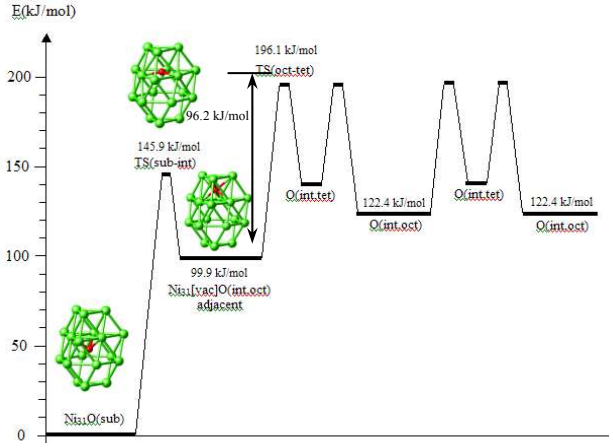

Figure 10. *Energetics of oxygen transport in nickel as determined from first-principles modeling.*

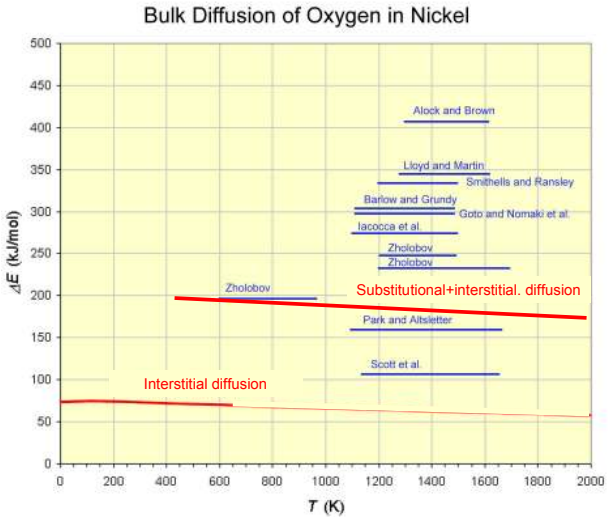

Figure 11. *Comparison of first-principles modeling predictions (red lines) and experimental data (blue lines) for oxygen diffusion in nickel. The modeling results are in good agreement with the experimental data of Zholobov and Park and Alstetter.*

Table IV. *Key Observations of SCC of A600-type Alloys and Their Implications*

Observation	Implication
Crack tips are sharp, consistent with embrittlement and moving crack fracture mechanics predictions for elastic-perfect plasticity	SCC occurs continuously via stable intergranular tearing and not by a discontinuous (crack-arrest-accumulate damage) process
Cracking is truly intergranular not along slip planes	Decohesion, not enhanced plasticity is responsible for crack growth
The crack growth rate shows a clear dependence with electrochemical potential around Ni/NiO	Crack growth rate is controlled by environmental processes (e.g. embrittler production, entry, and transport to the fracture process zone), not by mechanical variables. For hydrogen, the peak in rate near Ni/NiO may be a competition between H production via corrosion and H entry through an oxide film. For oxygen, the CGR likely decreases with increasing Ni stability, but it is unclear if the decrease in rate with increased NiO stability can be explained.
The crack growth rate of Alloy 600-type alloys is relatively insensitive to the applied stress intensity factor	
The apparent activation energy for steady state SCC is ~91.2 ±27.4 kJ/mol (this study), and is insensitive to changes in σ_{YS} or applied K_I (see Morton's paper these proceedings)	
For a given A600–type alloy, precipitation of chromium rich carbides (Cr_7C_3 or $Cr_{23}C_6$) produces slower crack growth rates	1.Cr depletion lowers the fugacity of H_2 produced via (Ni,Cr,Fe)O 2.Cr-rich carbides form protective Cr_2O_3 films, which lowers the amount of H_2 production 3. Cr_2O_3 sets a lower oxygen potential relative to NiO-type oxides and decreases oxygen uptake [47].
Over a wide stress intensity factor range, the crack growth rate is directly proportional to the applied stress intensity factor	$\dot{a} \propto K^1_{I,\,applied}$ small sample sizes or incomplete engagement bias apparent K dependence high (see Morton's paper these proceedings)
Factors that degrade the toughness of the starting material (e.g. plastic strain) increase the crack growth rate	$\dot{a} \propto 1/K_{IC}$, plastic strain, …

The schematic of an embrittled zone in front of a crack tip shown in Figure 12 is used to help illustrate the development of a crack growth rate equation. The crack growth rate, $\dot{a}$, is believed to be directly proportional to the embrittler supply rate (dC/dt), and dependent upon how the materials fracture toughness changes with concentration of the embrittling species (dJ_{IC}/dC). How J_{IC} varies with concentration is, of course, related to the concentration profile ahead of the crack tip and influences the tearing resistance (dJ_R/da) in a region very local to the crack tip.

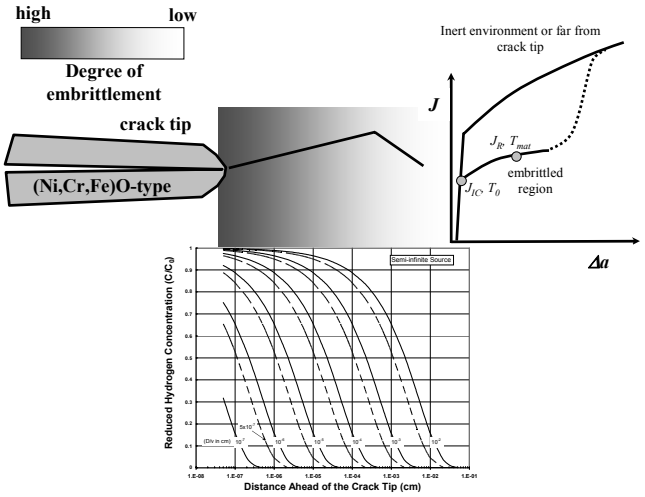

Figure 12. *Schematic illustration of an embrittled zone in front of an SCC crack tip, the local J-R curve (right) and the embrittler concentration profile (bottom).*

Crack advance occurs when the concentration of the embrittling species, C, lowers J_{IC} to the applied J. In this view of stress corrosion, the rate of crack advance is likely limited by the supply rate of the embrittling species since embrittler production and uptake are local to the crack tip region. Cracking occurs continuously (at constant applied J and constant environmental conditions) as the profile shown in Figure 12 is established and moves with the crack front. In other words:

$$\dot{a} \propto \frac{Supply\ rate\ of\ embrittler}{Concentration\ when\ J_{IC} \to J_{applied}} \tag{5}$$

The supply rate of the embrittling species is dependent on the strength of the source, the solubility, diffusivity, and how J_{IC} varies with embrittler concentration, i.e.

$$\dot{a} \propto \frac{embrittler\ source\ strength,\ solubility,\ diffusivity}{concentration\ when\ J_{IC} \to J_{applied}} \tag{6}$$

Noting that:

$$\begin{aligned} &source\ strength \to corrosion \\ &solubility, diffusivity \to effective\ permeability \\ &concentration\ for\ crack\ advance\ \propto J_{IC}\ and \propto 1/J_{applied} \end{aligned} \tag{7}$$

We can use (7) and (8) to write a steady state crack growth rate equation that describes the key parameters, i.e. the mechanical driving force ($J_{applied}$), corrosion ($f_{corrosion}$), material toughness (J_{IC}), and a temperature dependence (Q) that is relatively constant for A600-type alloys and independent of the $J_{applied}$ and J_{IC}.

$$\dot{a} = \frac{A_0\ J_{applied}\sqrt{f_{corrosion}}}{J_{IC}} \exp\left\{\frac{-Q_{H\ production} - Q_{H\ entry} - Q_{H\ effective\ diffusion} + \overline{V}_H \cdot \sigma_{yy}}{R \cdot T}\right\} \tag{8}$$

For engineering utility we: (1) convert from J to K, (2) allow an empirically determined K-dependence, K^n, (3) employ the effect of electrochemical potential for the fugacity dependence [13], and (4) utilize the activation energy determined from crack growth rate testing ($Q_{Effective}$):

$$\dot{a} = A_0 \cdot \frac{K_I^n}{K_{IC}} \cdot \left\{1 + b \cdot \exp\left[-0.5 \cdot \left(\frac{(\Delta EcP_{Ni/NiO} - x_0)}{c}\right)^2\right]\right\} \cdot \exp\left\{\frac{-Q_{Effective}}{R \cdot T}\right\} \tag{9}$$

Equation (9) is the general form that describes crack growth of A600-type alloys exposed to high temperature, high purity water. The effect of material toughness (K_{IC}) may be alternately described by a dependence on plastic strain or on yield strength, i.e. $K_{IC} \propto (\varepsilon_{plastic})^{-1}$ or $\propto (\sigma_{YS})^{-1}$ as others have shown [4, 59, 60].

Application of the Model – SCC of an Alloy 600 HAZ

A summary of the data used to fit to Equation 9 is given in Table V. The reported average crack growth rates were corrected to 100% crack front engagement and for out-of-plane growth. Since there were insufficient data to fit every parameter in the model independently, the data at 640°F (338°C) were used to determine the constant, b=3.604, and then the entire model and dataset were fit to both crack growth rate (i.e. linear space) and log crack growth rate (i.e. log space). Physically, b is the magnitude of the effect of the electrochemical potential. The parameters from each fitting method are given in Table VI, the fits are compared in Figure 13, and the linear space fit shown is shown in Figure 14.

Table V. *Summary of Alloy 600 HAZ Crack Growth Rate Data*

Temperature (°F)	Average K_I (ksi√in)	ΔEcP from Ni/NiO (mV)	Average Crack Growth Rate (mils/day)
550	36.40	28.20	0.086
550	36.60	28.20	0.099
600	41.00	8.90	0.573
600	41.10	8.90	0.509
640	40.10	-44.50	1.491
640	15.70	11.20	0.677
640	15.50	11.20	0.643
640	26.23	11.20	1.007
640	35.20	8.40	1.387
640	38.80	11.20	1.976
640	43.40	11.20	2.160
640	43.00	11.20	1.894
640	42.40	61.10	0.683
680	43.40	61.10	3.127
680	43.80	4.90	3.636

It is notable that fitting in linear space and log space produce very different values of the apparent activation energy for crack growth. Fitting in log space gives Q=136 kJ/mol, which is comparable to that reported in many other studies using a similar methodology (*i.e.* determining Q from the slope of a log(crack growth rate) vs. 1/T plot [61, 62]. However, fitting the data in linear space gives a significantly different Q of 91.2 kJ/mol. Understanding of the true activation energy for crack growth is important because: (1) is has a strong effect on extrapolated crack growth rates (2) it lends insight into the physical processes that are involved in stress corrosion cracking and (3) it gives insight into mechanistically based equation forms used to predict crack growth rates. The linear space fit is more applicable than the log space fit because: (1) it minimizes the error in the response that is physically significant, (2) it better predicts the 680°F (360°C) data where there is high confidence in the crack growth rate (Fig. 13) and (3) the Authors expect that both the 550°F (288°C) and 600°F (316°C) data may be biased low, since those cracks did not grow long enough to encounter the most susceptible microstructure in the HAZ. If the 550°F (288°C) and 600°F (316°C) data were shifted to the right, they would fall on the linear space fit but be over-predicted by the log space fit.

Table VI. *Fitted Parameters for the Alloy 600 HAZ Data*

	ln (A_0)	n	b	x_0 (mV)	c (mV)	Q (kJ/mol)
	Fitting in Linear Space					
Best Estimate	13.334	0.995	3.604	-11.33	43.36	91.2
95% Confidence	± 6.434	± 0.614	---	± 19.84	± 28.41	±27.4
	Fitting in Log Space					
Best Estimate	22.607	0.869	3.604	-15.61	42.79	136.0
95% Confidence	±3.729	±0.349	---	±20.71	±19.25	±18.2

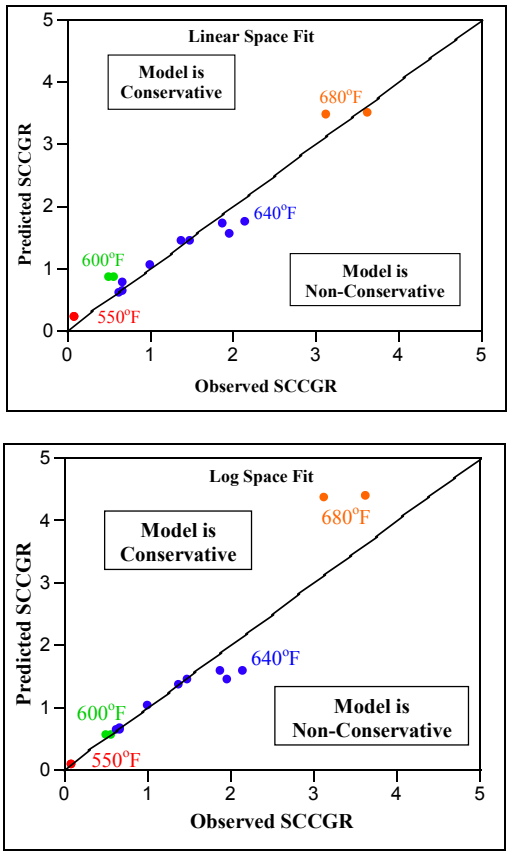

Figure 13. *Comparison of predicted vs. observed fits for crack growth (i.e. linear space fit – top) and log (crack growth) (i.e. the log space fit – bottom). Note the linear space fit is preferred as discussed in the text.*

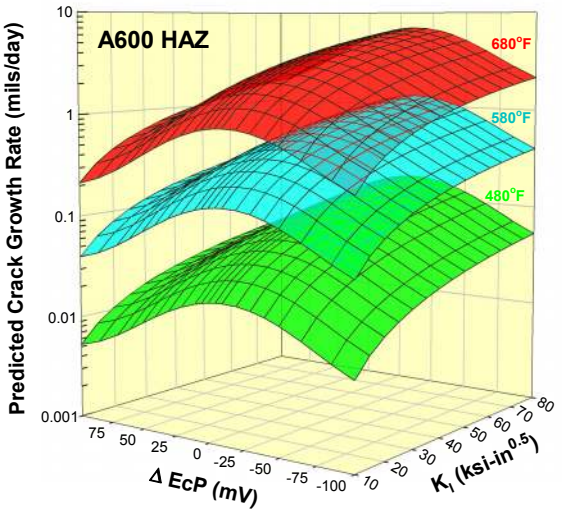

Figure 14. *Illustration of the predicted crack growth rates for Alloy 600 HAZ material as a function of potential, stress intensity factor, and temperature. Note 1 mil/day is ~1.0x10^{-6} m/hr or ~2.9x10^{-10} m/s.*

Conclusions

- Consistent with previous findings, analytical electron microscopy characterization of primary water crack tips shows that crack tips are sharp, truly intergranular, and there is no evidence of an increased dislocation density (*i.e.* a plastic strain gradient) in front of SCC crack tips. The implication of these findings is that embrittlement and decohesion, not enhanced plasticity is responsible for crack growth.
- Moving crack fracture mechanics of a crack growing through an elastic-perfectly plastic material accurately describe the experimentally observed crack tip opening displacements, giving credence to the notion that SCC is accurately described as stable intergranular tearing.
- Assessment of selected crack growth rate mechanisms suggests that SCC of nickel based alloys may occur via hydrogen embrittlement and be limited by the supply rate of hydrogen to the crack tip process zone.
- The concept of embrittler supply rate limited cracking is used to develop a mechanistically based equation of the form:

$$\dot{a} = A_0 \cdot \frac{K_I^n}{K_{IC}} \cdot \left\{ 1 + b \cdot \exp\left[-0.5 \cdot \left(\frac{(\Delta E c P_{Ni\,/\,NiO} - x_0)}{c} \right)^2 \right] \right\} \cdot \exp\left\{ \frac{-Q_{Effective}}{R \cdot T} \right\}$$

  This equation is suggested as being generally applicable to describe the SCC of A600-type metals exposed to high purity high temperature deaerated water.
- An example illustrating the use of the crack growth rate equation for Alloy 600 heat affected zone material shows a good to fit the data. However, it is notable that the choice of fitting in log space (as is commonly done) vice linear space yields very different apparent activation energies for crack growth. The linear space fit, which yields a Q of 91.2 kJ/mol ± 27.4 kJ/mol, preferred for the reasons discussed in the paper.

Acknowledgements

The Authors wish to thank Dr. D.R. Eno of Lockheed Martin who performed the statistical analysis of the data, Dr. T.L. Sham of Lockheed Martin for his assistance in the moving crack analyses, Ms. Michelle Othon of GE-GRC & Dr. Luke Brewer of Sandia National Laboratories who performed the electron backscatter diffraction work, Dr. Reza Najafabadi of Lockheed Martin, and Drs. Erich Wimmer & Jurgen Sticht of Materials Design Inc. who performed the atomistic modeling.

References

1. Vermilyea, D.A. *A Film Rupture Model for Stress Corrosion Cracking*. in *Stress Corrosion Cracking and Hydrogen Embrittlement of Iron Base Alloys*. 1973. Firminy, France: NACE.
2. Ford, F.P. *The Crack-Tip System and Its Relevance to the Prediction of Cracking in Aqueous Environments*. *Environment-Induced Cracking of Metals*. 1988. Kohler, WI: NACE.
3. van Leewen, H.P., *Quantitative Models of Hydrogen-Induced Cracking of High Strength Steel*, in *Reviews on Coatings and Corrosion*. 1979, Tel-Aviv Scientific Publications, p. 5-93.
4. Hall, M.M. and D.M. Symons. *HACF Model for Low Pot. SCC of Ni-Cr-Fe Alloys*. in *Chemistry and Electrochemistry of Corrosion and SCC*. 2001. New Orleans, TMS.
5. Hall, M.M., *Environment-Assisted Creep Fracture Model for Primary Water Stress Corrosion Cracking of Alloy 600*, in *EPRI Workshop on Alloy 600*. 1997, Daytona Beach, FL.
6. Lewis, N., B.W. Bussert, and M.L. Bunch. *Cross-Sectional AEM Analysis of SCC Cracks*. in *EPRI Steam Generator IGA/SCC Workshop*. 1992. San Antonio, TX: EPRI.
7. Lewis, N., et al. *Stress Corrosion Crack Growth Rate Testing and Electron Microscopy of Alloy 600 as a Function of Pourbaix Space and Microstructure*. in *Chemistry and Electrochemistry of Corrosion and SCC* 2001. New Orleans, LA: TMS.
8. Somerday, B.P., L.M. Young, and R.P. Gangloff, *Crack Tip Mechanics Effects on Environment-Assisted Cracking of Beta-Titanium Alloys in Aqueous NaCl.* Fatigue Fract. Eng. Mater. Struct., 2000. **23**: p. 39-58.
9. Deshais, G. and S.B. Newcomb. *The Influence of Microstructure on the Formation of Stress Corrosion Cracks in 7XXX Series Aluminum Alloys*. in *7th International Conference on Aluminum Alloys: Their Physical and Mechanical Properties*. 2000. Charlottesville, VA: Trans Tech Publications.
10. Cooper, K.R. and R.G. Kelly. *Measurement and Modeling of Crack Conditions During the Environment-Assisted Cracking of An Al-Zn-Mg-Cu Alloy*. in *Chemistry and Electrochemistry of Stress Corrosion Cracking*. 2001. New Orleans, LA: TMS.
11. Shih, C.F., *Relationship between the J-Integral and the Crack Opening Displacement for Stationary and Extending Cracks*. J. of the Mech. Phys. Solids, 1981. **29**: p. 305-326.
12. Rice, J.R., W.J. Drugan, and T.-L. Sham. *Elastic-Plastic Analysis of Growing Cracks*. in *Fracture Mechanics: Twelfth Conference, ASTM STP 700*. 1980.
13. Morton, D.S. *Primary Water SCC Understanding and Characterization Through Fundamental Testing in the Vicinity of the Nickel/Nickel Oxide Phase Transition*. in *10th International Conference on Environmental Degradation of Materials in Nuclear Power Systems*. 2001. Lake Tahoe, NV: NACE.
14. Young, G.A., N. Lewis, and D.S. Morton. *The Stress Corrosion Crack Growth Rate of Alloy 600 Heat Affected Zones Exposed to High Purity Water*. in *Nuclear Regulatory Commission Conference on Vessel Head Penetration Inspection, Cracking, and Repairs*. 2003. Gaithersburg, MD: NRC.
15. Hohenburg, P. and W. Kohn, Phys. Rev., 1964. **136**(B864).
16. Kohn, W. and L.J. Sham, Phys. Rev., 1965. **140**(A1133).
17. Wang, Y. and J.P. Perdew, Phys. Rev. B, 1991. **54**(13298).
18. Perdew, J.P. and Y. Wang, Phys. Rev. B, 1992. **45**(13244).
19. Blochl, P.E., Phys. Rev. B, 1994. **50**(17): p. 953.
20. Parlinski, K., Z.Q. Li, and Y. Kawazoe, Phys. Rev. Letters, 1997. **78**(4063).
21. Thompson, C.D., et al. *Prediction of PWSCC in Nickel Base Alloys Using Crack Growth Rate Models*. in *Seventh International Symposium on Environmental Degradation of Materials in Nuclear Power Systems - Water Reactors*. 1995. Breckenridge, CO: ANS/NACE/TMS.
22. Young, G.A. and J.R. Scully, *The Effects of Test Temperature, Temper, and Alloyed Copper on the Hydrogen-Controlled Crack Growth Rate of an Al-Zn-Mg-(Cu) Alloy.* Met. Trans. A, 2002. **33A**: p. 1167-1181.
23. Morton, D.S., et al. *The Influence of Dissolved Hydrogen on Nickel Alloy SCC: A Window to Fundamental Insight - #01117*. in *Corrosion*. 2001: NACE.
24. Rosecrans, P.M. and D.J. Duquette, *Formation Kinetics and Rupture Strain of Ni-Cr-Fe Alloy Corrosion Films Formed in High Temp. Water.* Met. Trans A., 2001. **32A**: p. 3015-3021.
25. Brucelle, O., et al. *A Study of Corrosion Mechanisms and Kinetics of Alloy 718 in PWR Primary Water*. in *Ninth International Symposium on Environmental Degradation of Materials in Nuclear Power Systems-Water Reactors*. 1999: TMS.
26. Kishimoto, N., et al., *Hydrogen Diffusion and Solution at High Temperatures in 316L Stainless Steel and Nickel-Base Heat-Resistant Alloys.* J. Nuclear Mat., 1985. **127**: p. 1-9.

27. Louthan, M.R., J.A. Donovan, and G.R. Caskey, *Hydrogen Diffusion and Trapping in Nickel.* Acta Met., 1975. **23**: p.745-749.
28. Volkl, J. and G. Alefeld, *Diffusion of Hydrogen in Metals*, in *Hydrogen in Metals*, G. Alefeld and J. Volkl, Editors. 1978, Springer Verlag: New York. p. 321-348.
29. Rota, E., et al., *Measurements of Surface and Bulk Properties for the Interaction of Hydrogen with Inconel 600.* J. Nucl. Mat., 1982. **111&112**: p. 233-239.
30. Totsuka, N. and Z. Szklarska-Smialowska. *Hydrogen Induced IGSCC of Ni-Containing FCC Alloys in High Temperature Water*. in *Proceedings of the Third International Conference on Environmental Degradation of Materials in Nuclear Power Systems*. 1987: TMS.
31. Yonezawa, et al. *Electron Micro-autoradiographic Observation of Tritium Distribution on Alloy X750*. in *Proceedings of the International Symposium on Plant Aging and Life Predictions of Corrodible Structures*. 1995. Sapporo, Japan.
32. Magnin, T. *Corrosion Deformation Interaction During Stress Corrosion Cracking of Alloy 600 in Primary Water*. in *The Sixth International Symposium on Environmental Degradation of Materials in Nuclear Power Systems-Water Reactors*. 1993: TMS.
33. Bellanger, G. and J.J. Rameau, *Behavior of 316 Ti SS in D_2O with Chloride.* J. Mat. Sci., 1997. **32**: p. 4355-4376.
34. Hall, M.M. *Thermally Activated Dislocation Creep Model for Primary Water Stress Corrosion Cracking of NiCrFe Alloys*. in *Proceedings of International Symposium on Plant Aging and Life Prediction of Corrodible Structures*. 1995. Sapporo, Japan.
35. Bruemmer, S.M. and L.E. Thomas. *Insights into Environmental Degradation Mechanisms from High-Resolution Characterization of Crack Tips*. in *Chemistry and Electrochemistry of SCC*. 2001. New Orleans: TMS.
36. Rios, R., et al., *Critical Analysis of Alloy 600 Stress Corrosion Cracking Mechanisms in Primary Water.* Met. Trans. A, 1995. **26A**: p. 925-939.
37. Birnbaum, H.K. *Mechanisms of Hydrogen Related Fracture of Metals*. in *Hydrogen Effects on Material Behavior*. 1990. Jackson Hole, WY: TMS.
38. Sofronis, P., et al. *Recent Advances in the Study of Hydrogen Embrittlement at the University of Illinois*. in *Hydrogen Effects on Material Behavior and Corrosion Deformation Interactions*. 2003. Jackson Hole, WY: TMS.
39. Birnbaum, H.K., *Hydrogen Effects on Deformation and Fracture.* MRS Bulletin, 2003. **28**(7): p. 479-485.
40. Hall, M.M., W.C. Moshier, and D.J. Paraventi. *Hydrogen Assisted Fracture Model Predictions for Alloy 600 PWSCC*. in *Conference on Vessel Head Penetration Inspection, Cracking and Repair*. 2003. Gaithersburg, MD: NRC.
41. Scott, P. and M. LeCalvar. *Some Possible Mechanisms of Intergranular SCC of Alloy 600 in PWR Primary Water*. in *Specialists Meeting on Environmental Degradation of Alloy 600*. 1996. Palo Alto, CA: EPRI.
42. Scott, P.M. *An Overview of Internal Oxidation as a Possible Explanation of Intergranular Stress Corrosion Cracking of Alloy 600 in PWR's*. in *Ninth International Symposium on Environmental Degradation of Materials in Nuclear Power Systems-Water Reactors*. 1999. Newport Beach, CA: TMS.
43. Scott, P.M. and M. LeCalvar. *Some Possible Mechanisms of Intergranular SCC of Alloy 600 in PWR Primary Water*. in *Sixth International Symposium on Environmental Degradation of Materials in Nuclear Power Systems*. 1993. San Diego, CA: TMS.
44. Gendron, T.S., et al. *Internal Oxidation as a Mechanism for Steam Generator Tube Degradation*. in *3rd Conference on Steam Generators and Heat Exchangers*. 1998. Toronto, ON, CNS.
45. Newman, R.C., T.S. Gendron, and P.M. Scott. *Internal Oxidation and Embrittlement of Alloy 600*. in *Ninth International Symposium on Environmental Degradation of Materials in Nuclear Power Systems*. 1999. Newport Beach, CA: TMS.
46. Gourgues, A.F., P.M. Scott, and E. Andrieu. *A Study of the Mechanism of Primary Water Stress Corrosion Cracking of Alloy 600*. in *Seventh International Symposium on Environmental Degradation of Materials in Nuclear Power Systems - Water Reactors*. 1995. Breckenridge, CO: NACE.
47. Staehle, R.W. and Z. Fang. *Comments on a Proposed Mechanism of Internal Oxidation for Alloy 600 as Applied to Low Potential SCC*. in *Ninth International Conference on Environmental Degradation of Materials in Nuclear Power Systems - Water Reactors*. 1999. Newport Beach, CA: TMS.
48. Alcock, C.B. and P.B. Brown, *Physiochemical Factors in the Dissolution of Thoria in Solid Ni.* Met. Sci. J., 1969. **3**: p. 116.
49. Lloyd, G.J. and J.W. Martin, *The Diffusivity of Oxygen in Nickel Determined by Internal Oxidation of Dilute Ni-Be Alloys.* Metal Science Journal, 1972. **6**: p. 7-11.
50. Smithells, C.J. and C.E. Ransley, *The Diffusion of Gases Through Metals: III-The Degassing of Nickel and the Diffusion of Carbon Monoxide Through Nickel.* Proceedings of the Royal Society, 1936. **A155**: p. 195-212.
51. Barlow, R. and P.J. Grundy, *The Determination of the Diffusion Constants of Oxygen in Nickel and Gamma-Iron by an Internal Oxidation Method.* J. of Mat. Sci., 1969. **4**: p. 797-801.
52. Iacocca, R.G. and D.A. Woodford, *The Kinetics of Intergranular Oxygen Penetration in Nickel and its Relevance to Weldment Cracking.* Met. Trans A., 1988. **19A**: p. 2305-2313.
53. Zholobov, S.P. and M.D. Malev, *Diffusion of Oxygen in a Metal in Electron Bombardment of the Surface.* Soviet Physics-Technical Physics, 1971. **16**: p. 488-494.
54. Park, J.W. and C.J. Alstetter, *The Diffusion and Solubility of Oxygen in Solid Nickel.* Met. Trans A., 1987. **18A**: p. 43-50.
55. Goto, S., K. Nomanki, and S. Koda, *Internal Oxidation of Nickel Alloys Containing a Small Amount of Chromium.* J. Jap. Inst. Metals, 1967. **31**(1967): p. 600-606.
56. Wolverton, C., V. Ozolins, and M. Asta, *Hydrogen in Aluminum: First Principles Calculations of Structure and Thermodynamics.* Phys. Rev. B, 2004. **69**.
57. Young, G.A. and J.R. Scully, *The Diffusion and Trapping of Hydrogen in High Purity Aluminum.* Acta Met., 1998. **46**(18): p. 6337-6349.
58. Young, G.A., et al. *Applications of Ab Initio Modeling. MedeA User's Group Meeting*. 2004. Orcas Island, WA.
59. Speidel, M.O. and R. Magdowski. *Stress Corrosion Cracking of Nickel Base Alloys in High Temperature Water*. in *Sixth International Symposium on Environmental Degradation of Materials in Nuclear Power System*. 1993. San Diego, CA: TMS.
60. Moshier, W.C. and C.M. Brown. *Effect of Cold Work and Processing Orientation on the SCC Behavior of A600*. in *NACE 99*. 1999: NACE.
61. *Materials Reliability Program Crack Growth Rates for Evaluating PWSCC of Alloy 82, 182, and 132 Welds*, J. Hickling, Ed. 2004, EPRI.
62. Attanasio, S.A., et al. *Stress Corrosion Crack Growth Rates of Alloy 182 and 82 Welds*. in *NRC Conference on Vessel Head Penetration Inspection, Cracking, and Repairs*. 2003. Gaithersburg, MD: NRC.